Decoupling behavior in ^{132}La

Vinod Kumar* and Pragya Das†
Physics Department, Indian Institute of Technology Bombay, Powai, Mumbai 400076, India

S. Lakshmi, P. K. Joshi, and H. C. Jain
Tata Institute of Fundamental Research, Homi Bhabha Road, Mumbai 400005, India

R. P. Singh, R. Kumar, S. Muralithar, and R. K. Bhowmik
Inter-University Accelerator Centre, Aruna Asaf Ali Marg, New Delhi 110067, India
(Received 3 September 2008; revised manuscript received 16 June 2010; published 4 November 2010)

Heavy-ion fusion reactions ^{122}Sn(^{14,15}N, xn)^{132}La have been utilized for the lifetime measurements using the recoil distance method. The lifetimes of seven low-lying excited states were obtained. In addition, the lifetimes of two states belonging to a band, which was identified as a decoupled band, were obtained. The decoupling behavior in ^{132}La has been theoretically investigated using the particle-rotor model in the model space of $\pi h_{11/2}$ and ($\nu s_{1/2}$, $\nu d_{3/2}$). The pseudospin coupling model was also utilized to understand the decoupling behavior in terms of the valence-particle configuration $\pi h_{11/2}(\Omega_\pi = \frac{1}{2}) \otimes \nu[\widetilde{411}](\Omega_\nu = \frac{1}{2}, \frac{3}{2})$, and a reasonable agreement with the experiment was obtained.

DOI: 10.1103/PhysRevC.82.054302 PACS number(s): 23.20.Lv, 21.10.Tg, 27.60.+j, 25.70.−z

I. INTRODUCTION

The phenomenon of chirality has been the main focus of attention for studying the odd-odd nuclei in the mass region near 130 [1]. The decoupled bands, though experimentally found in many nuclei, such as ^{128}Pr [2], ^{130,132}Pr [3], and ^{134}Pm [4], have not been theoretically investigated very well. In the upper rare-earth region, the well-studied cases of double decoupling are ^{176}Re [5] and ^{186}Ir [6].

The ground state (2^-) of ^{132}La and an isomeric state (6^-) were originally identified by the electron conversion measurement [7]. Two bands based on the particle configurations $\pi h_{11/2} \otimes \nu h_{11/2}$ and $\pi g_{7/2} \otimes \nu h_{11/2}$, were identified by Oliveira *et al*. [8]. An extensive study of the $\pi h_{11/2} \otimes \nu h_{11/2}$ band and its chiral partner band was done by Starosta *et al*. [1,9,10]. In our earlier experimental measurements [11], we made a definite spin assignment to the bandhead of the chiral band by identifying two new transitions of energies, 38 and 351 keV. Similar results were also reported by Timár *et al*. [12]. We also found a new negative-parity band consisting of $E2$ transitions [11]. This band was identified as a decoupled band because the energy-level spacings were very similar to the ground-state bands of the neighboring nuclei ^{130}Ba and ^{131}La. Recently, Grodner *et al*. [13] measured the lifetimes of states belonging to the chiral partner bands and compared their results with theoretical calculations based on the core quasiparticle coupling model.

The main focus of the work presented here is to ascertain the decoupled nature of the newly found negative-parity band [11] and to further investigate its properties. We performed two lifetime experiments in the picosecond range using the recoil distance method (RDM). A moderate value of the axial deformation parameter ($\beta = 0.18 \pm 0.02$) was obtained for the decoupled band from the lifetime measurements. The behavior of the decoupled band was explained using the particle-rotor model and the pseudospin coupling model. In both these models, we considered the valence proton configuration as $(\pi h_{11/2})\Omega_\pi = \frac{1}{2}$. However, the valence neutron configuration used was $(\nu d_{3/2}s_{1/2})\Omega_\nu = \frac{1}{2}, \frac{3}{2}$ in the particle-rotor model, and $[\widetilde{411}]\Omega_\nu = \frac{1}{2}, \frac{3}{2}$ in the pseudospin coupling model. To do a systematic investigation, we also performed the calculations for the neighboring nuclei ^{131}La and ^{131}Ba. Both the models provided a reasonable agreement with the experimental data.

II. EXPERIMENTAL DETAILS

The first lifetime measurement was performed at the Tata Institute of Fundamental Research (TIFR), Mumbai. The ^{14}N beam, delivered by the Pelletron accelerator at the energy of 62 MeV, was focused on a ^{122}Sn target. The high recoil velocity of the residues is an important parameter for the RDM measurement. In the experiment done at TIFR, the velocity of the residues was low ($\simeq 0.003c$). To obtain higher velocities of the residues, we performed another experiment with a ^{15}N beam of 83 MeV on a ^{122}Sn target at the Inter-University Accelerator Centre (IUAC), New Delhi. In this experiment, ^{132}La was populated through the $5n$ reaction channel. The gain in recoil velocity was due to the higher mass and energy of the projectile. In both the experiments, the Sn foil of thickness 0.5 mg/cm^2 was prepared by rolling along with a supporting material Au of thickness 2 mg/cm^2. The difficulty of making a self-supporting Sn target of thickness below 1 mg/cm^2 was avoided by using the supporting material. The stopper was Au of thickness 5 mg/cm^2. The flatness of both the target and the stopper was achieved by the stretching method. The target and the stopper were mounted inside the plunger

*Present address: University of Delhi, India.
†pragya@phy.iitb.ac.in

setup and the distance between them was measured by the capacitance measurement technique described by Alexander and Forster [14]. In both experiments the beam current was 3–4 pnA. For each target-stopper distance the data were collected for roughly 3 h.

The plunger setup at TIFR [15] consisted of a fixed target mounting plate and a movable stopper assembly. The separation between the target and the stopper could be manually adjusted by a micrometer screw from outside the vacuum chamber. A standard coaxial high-purity germanium detector (HPGe) at 90° and a four-element Clover HPGe detector at 30° with respect to the beam direction were used. The detectors were placed at the distance of 20 cm from the target position. The dimension of the standard HPGe detector and each section of the Clover HPGe detector were roughly the same, and was 5 cm in diameter and 6 cm in length. The data were collected in the singles mode. The target-stopper separation was varied between 6 and 1650 μm.

The experimental setup at IUAC consisted of a plunger inside the multidetector array. The multidetector facility, called the γ-detector array (GDA) [16], consisted of 12 Compton-suppressed coaxial HPGe detectors, whose size was similar to the coaxial HPGe detector used in the TIFR experiment. These HPGe detectors were placed at a distance of 20 cm from the target, and were oriented at the angles of (θ) $\pm 50°$, $\pm 98°$, and $\pm 144°$ with respect to the beam direction. They were positioned in two planes that made an angle of $\pm 25°$ with the horizontal plane. A set of 14 BGO detectors in the honeycomb structure, seven above and seven below the horizontal plane, were placed as the multiplicity filter. The target-stopper assembly was housed in the plunger vacuum tube. The stopper could be moved by dc motors, which were controlled remotely by a personal computer. The minimum distance achieved in our experiment was 5.7 μm. In total, 16 distances were covered ranging from 5.7 μm to 6620 μm. The γ-γ coincidence data were recorded in the event-by-event mode, called the list mode, when two or more detectors were fired. The energy spectra of individual detectors were also recorded in the singles mode.

III. DATA ANALYSIS AND RESULT

The singles data collected at TIFR were analyzed after adding the spectra from all the sections of the Clover detector placed at 30° with respect to the beam direction. The data were normalized with respect to the spectrum of the 90° detector. For the experiment done at IUAC, the list mode data were analyzed by making $E_\gamma(\theta)$ versus E_γ(all) matrices. Two such matrices were constructed for $\theta = 50°$ and $\theta = 144°$. For the coincident γ rays, E_γ(all) included events at any detector position. The analysis of a particular γ ray observed at the angle θ was done either by taking the total projection or specific energy gates on the E_γ(all) axis. The data were calibrated with the radioactive sources ^{152}Eu and ^{133}Ba. As the Doppler-shifted and the unshifted peaks were close in energy, there was no need to do the efficiency correction for finding the intensity ratio R($\equiv \frac{I_0}{I_0+I_s}$). The areas (intensity) of shifted (I_s) and unshifted (I_o) peaks were measured by fitting the peaks to a Gaussian of adjustable heights, while constraining the widths. The RADWARE software [17] was utilized for analyzing the energy spectra. The peak widths were estimated by fitting the fully shifted and unshifted peaks. The recoil velocity of the residues were measured from the peak positions of the shifted and the unshifted peaks, and was found to be $0.0030c \pm 0.0005c$ and $0.0100c \pm 0.0005c$ for the TIFR and IUAC experiments, respectively. The width of the shifted peak was large because of the velocity distribution of the recoiling nuclei. The peak width was measured as a fraction of the photopeak energy and was found to be about 15% and 5% for the TIFR and IUAC experiments, respectively. The width of the shifted peak was more for the TIFR experiment than that for the IUAC experiment. The larger width obtained in the TIFR experiment was mainly due to two reasons. First, the straggling in the energy loss is higher at low recoiling velocity of the residues. Second, the Doppler broadening is more for the Clover detector because the position angles of each of the sections of the Clover was not exactly 30°, causing the effective opening angle to be much more than that of the coaxial HPGe detector used in the IUAC experiment.

The lifetime of the energy states was determined using the fitting procedure given in the Appendix.

Figure 1 gives the relevant part of the decay scheme of ^{132}La [11]. The red-colored transitions were studied in the present RDM analysis.

Figure 2 shows the example of shifted and unshifted peaks for 227-, 288-, 414-, and 557-keV γ lines from the TIFR experiment. These results were obtained from the singles data. The corresponding decay curves are shown in Fig. 3. The lifetimes of many states could not be determined, either because of poor statistical quality of the data or the presence of overlapping peaks.

The γ-γ coincidence data from the IUAC experiment was used to generate the projected spectra by gating on both shifted as well as unshifted components of various energy peaks. Such spectra, shown in Fig. 4, exhibited the shifted and unshifted components of 161-, 170-, 203-, 279-, 312-, 320-, 351-, 414-, 482-, and 557-keV transitions. The corresponding decay curves are shown in Fig. 5. The lifetimes for the

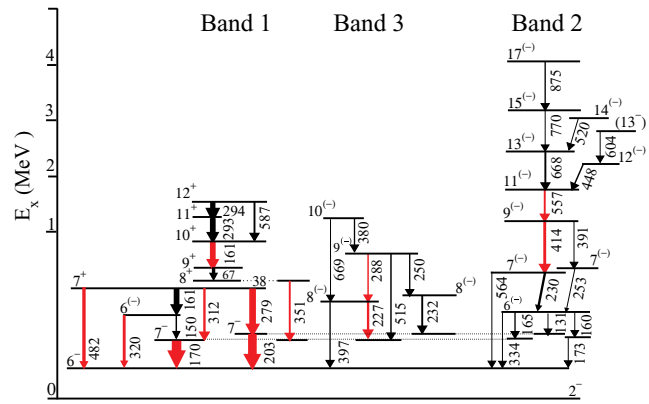

FIG. 1. (Color online) Partial level scheme of ^{132}La from our earlier work [11]. The red-colored γ transitions were studied in the present RDM analysis.

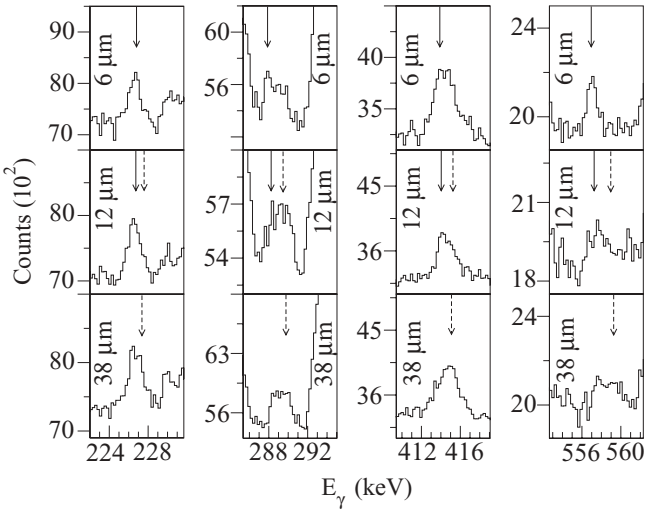

FIG. 2. Energy spectra for the transitions 227, 288, 414, and 557 keV obtained in the RDM experiment performed at TIFR. The distance mentioned in the units of μm is the target-stopper separation. Solid arrow indicates the position of the unshifted peak and the dashed arrow represents the shifted peak observed in a detector positioned at an angle of 30° with respect to the beam direction.

states decaying through γ transitions 227 and 288 keV could not be determined. This was because the transitions with very close energy values 230 and 293 keV were present in the projected spectrum with gate on 170 keV. For example, when the spectrum of the 144° detector was analyzed, the shifted peak of the 230-keV transition appeared at 228 keV. Similarly, in the spectrum of the 50° detector the shifted peak of the 227-keV transition appeared at 229 keV. This kind of contamination was much less in the TIFR spectrum because of the low recoil velocity of the residues, resulting in the smaller separation between the shifted and unshifted peaks. Table I lists the results of both the RDM experiments performed at TIFR and IUAC. The quoted error incorporates the fitting error and the error in the average velocity of the recoils.

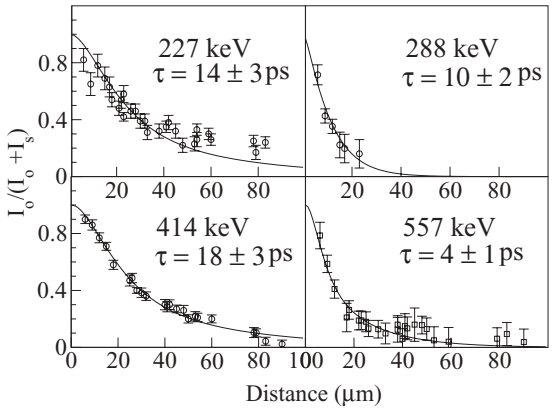

FIG. 3. Decay curves as a function of target-stopper separation "D" for the transitions 227 keV ($8^{(-)} \rightarrow 7^{-}$), 288 keV ($9^{(-)} \rightarrow 8^{(-)}$), 414 keV ($9^{(-)} \rightarrow 7^{(-)}$), and 557 keV ($11^{(-)} \rightarrow 9^{(-)}$) obtained from the RDM experiment at TIFR.

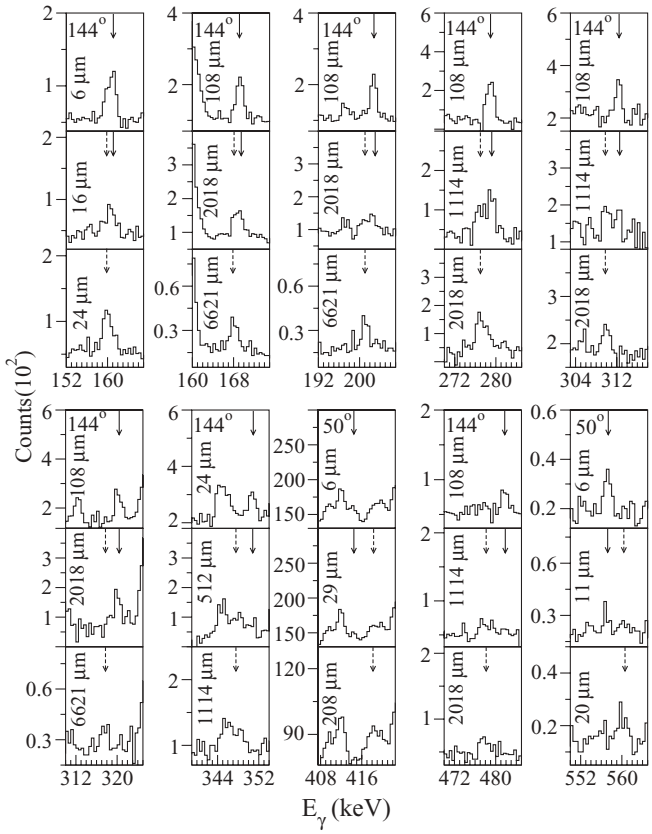

FIG. 4. Energy spectra for the transitions 161, 170, 203, 279, 312, 320, 351, 414, 482, and 557 keV obtained in the RDM experiment performed at IUAC. The distance mentioned in the units of μm is the target-stopper separation. The solid arrow indicates the position of the unshifted peak and the dashed arrow represents the shifted peak, observed at the designated angles with respect to the beam direction.

The latter was approximated to 15% for the TIFR experiment and 5% for the IUAC experiment as mentioned earlier. The last column of the table gives the gating transitions used for generating the projected spectra shown in Fig. 4 for the IUAC experiment.

IV. THEORETICAL INTERPRETATION AND DISCUSSION

A. Low-lying states

The lifetime values for the states $6^{(-)}$, 7^{-}, 7^{+}, and 8^{+} were found to be quite high (see Table I). Therefore they can be called isomeric states.

B. Band 2

A new negative-parity band, called band 2 in Fig. 1, was entirely built from our data [11]. We identified the bandhead as $7^{(-)}$ and a sequence of $E2$ transitions up to $17^{(-)}$. This band was identified as a decoupled band because the energy spacings between the levels were very similar to the ground-state band of the neighboring nuclei ^{131}La and ^{130}Ba, as shown in Fig. 6. Below $7^{(-)}$, the energy levels were connected to the isomeric state 6^{-} and the ground state 2^{-} by many decay paths. Assuming the axial deformation of the nucleus, the

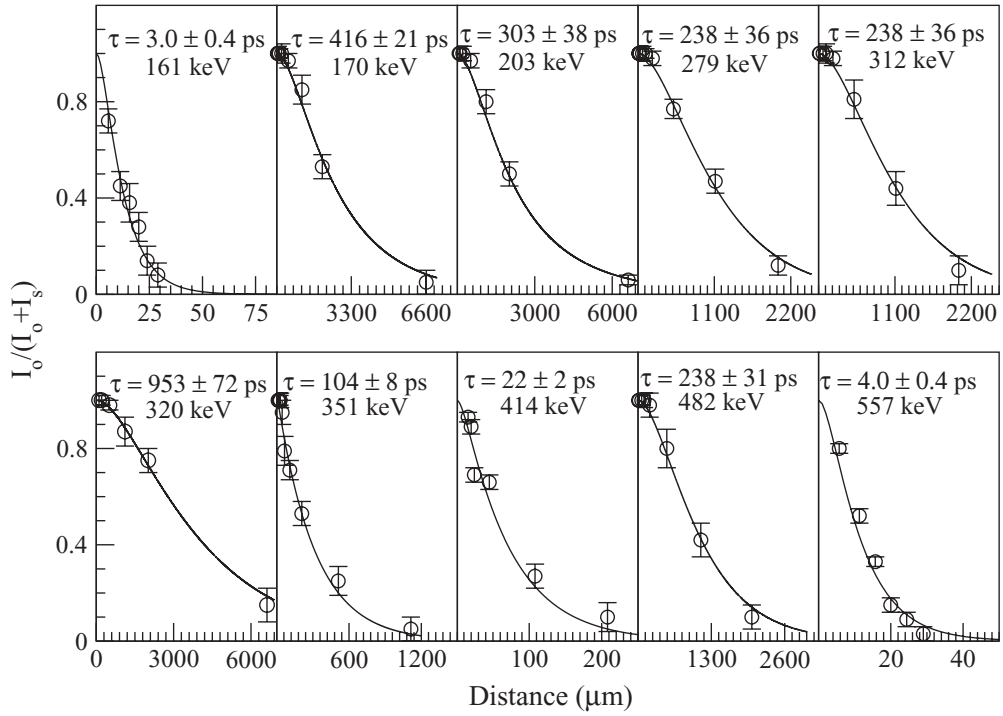

FIG. 5. The decay curves as a funtion of target-stopper separation "D" for the transitions 161 keV ($10^+ \rightarrow 9^+$), 170 keV ($7^- \rightarrow 6^-$), 203 keV ($7^- \rightarrow 6^-$), 279 keV ($7^+ \rightarrow 7^-$), 312 keV ($7^+ \rightarrow 7^-$), 320 keV ($6^{(-)} \rightarrow 6^-$), 351 keV ($8^+ \rightarrow 7^-$), 414 keV ($9^{(-)} \rightarrow 7^{(-)}$), 482 keV ($7^+ \rightarrow 6^-$), and 557 keV ($11^{(-)} \rightarrow 9^{(-)}$) obtained from the IUAC experiment.

deformation parameter β was calculated from the measured lifetime using the following formulas [18,19]: the decay rate in s^{-1}

$$T(E2) = 1.225 \times 10^9 E_\gamma^5 B(E2), \tag{1}$$

the reduced transition probability in e^2 fm

$$B(E2) = \frac{5}{16\pi} Q_0^2 |\langle I_i K 20 \mid I_f K\rangle|^2, \tag{2}$$

and the intrinsic quadrupole moment

$$Q_0 = \frac{3}{\sqrt{5\pi}} ZeR^2\beta. \tag{3}$$

Here E_γ is the energy of the γ ray in MeV, Z is the atomic number, and R is the nuclear radius which is taken to be equal to $1.2A^{1/3}$ fm. The Clebsch-Gordan coefficient $\langle I_i K 20 \mid I_f K\rangle$ represents the coupling of angular momenta, where I_i and I_f are the initial and final spin values, respectively. The value of K was taken to be zero because the decoupled band arises when the angular momenta are rotation aligned (i.e., the K value should be small). From our experimental

TABLE I. Mean lifetimes obtained from the RDM experiments.

Excitation energy E_x (keV)	Initial spin	γ energy E_γ(keV)	Mean lifetime of energy states (ps)		Gates (IUAC Experiment) (keV)
			(TIFR expt.)	(IUAC expt.)	
358	7^-	170		416 ± 21	351, 312
391	7^-	203		303 ± 38	279
508	$6^{(-)}$	320	855 ± 193	953 ± 72	161, 67
585	$8^{(-)}$	227	14 ± 3		
670	7^+	279		238 ± 36	203
670	7^+	312	222 ± 38	238 ± 36	170
670	7^+	482	222 ± 38	238 ± 31	161, 67
709	8^+	351		104 ± 8	170
873	$9^{(-)}$	288	10 ± 2		
937	10^+	161		3.0 ± 0.4	482, 279
1166	$9^{(-)}$	414	18 ± 3	22 ± 2	Total projection
1723	$11^{(-)}$	557	4 ± 1	4.0 ± 0.4	230, 414, 391

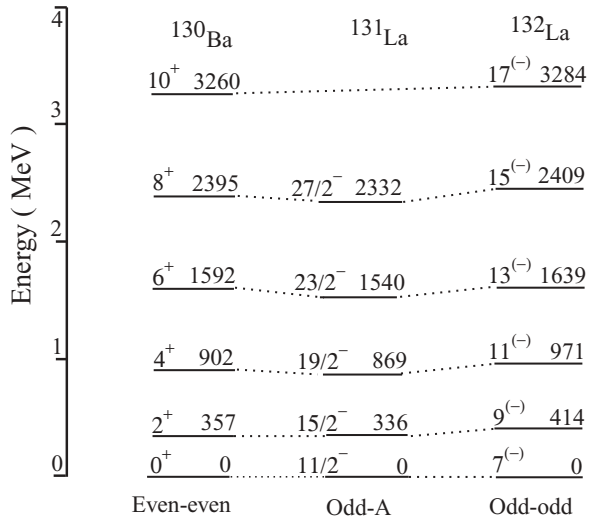

FIG. 6. The energy levels of the decoupled band in ^{132}La and ^{131}La in comparison with the even-even nucleus ^{130}Ba.

results of lifetimes for $9^{(-)}$ and $11^{(-)}$ states (Table I), the average value of β was found to be 0.18 ± 0.02. The value of β did not change significantly when $K = 1$ was considered.

We performed the particle-rotor model [20] calculations. The axial deformation parameter β was chosen to be 0.18, while the triaxial deformation parameter γ was taken to be zero. Since there was a very good similarity between the ground-state band based on $\pi h_{11/2}$ in ^{131}La and the decoupled band in ^{132}La (Fig. 6), the valence proton in $h_{11/2}$ was an obvious choice for our calculation. For the valence neutron configuration, the Nilsson energy levels at the deformation value $\beta = 0.18$ indicated the presence of $d_{3/2}$ and $s_{1/2}$ positive-parity orbits near $N \sim 75$. In the neighboring nucleus ^{131}Ba, the ground-state band was indeed identified as $(\nu d_{3/2}s_{1/2})$ by earlier workers [21]. We therefore used the valence particle configurations $(\pi h_{11/2}, \Omega_\pi = \frac{1}{2})$ and $(\nu d_{3/2}s_{1/2}, \Omega_\nu = \frac{1}{2}, \frac{3}{2})$ for ^{131}La, ^{131}Ba, and ^{132}La. In this model, the calculation for the odd-odd nucleus is performed by considering $K \equiv \Omega_\pi \pm \Omega_\nu$. The slight difference in the masses of ^{131}La, ^{131}Ba, and ^{132}La was ignored and the same values of moment of inertia parameters $J_0 = 7.7\hbar^2$ MeV^{-1} and $J_1 = 83.3\hbar^4$ MeV^{-3} in the Harris expansion were utilized for the entire calculations. These values of J_0 and J_1 were obtained from the ground-state band of the even-even core nucleus ^{130}Ba. The calculation was performed using the two-quasiparticle-rotor model. Similar calculations were performed for ^{131}La and ^{131}Ba using a one-quasiparticle-rotor model. The results, designated as "The. I" are presented in Figs. 7(a), 7(b), and 7(c) for ^{132}La, ^{131}La, and ^{131}Ba, respectively.

In the pseudospin coupling model, as suggested by Bohr *et al*. [22], one can identify the pseudospin singlet and doublet states in the Nilsson energy-level diagram. Kreiner [23] has used the concept of pseudospin to explain the decoupling behavior in nuclei in the mass region $A \sim 180$. Using the same prescription, we have performed the calculation by identifying the pseudospin doublet states $[\widetilde{411}\frac{1}{2}]$, $[\widetilde{411}\frac{3}{2}]$ for the valence neutron. However, for the valence proton, we have assumed the same configuration $(\pi h_{11/2}, \Omega_\pi = \frac{1}{2})$, as was used in the particle-rotor model. To calculate the energy eigenvalues, for the odd-odd nucleus ^{132}La, the 4×4 Coriolis matrix for the configuration space $\{\Omega_\nu = \frac{3}{2}, \frac{1}{2}\} \otimes \{\Omega_\pi = \frac{1}{2}\} = \{K = 2, 1, 1, 0\}$ can be written as

$$A(I)\begin{pmatrix} I(I+1)-2^2 & -a_p[(I-1)(I+2)]^{1/2} & -a_p[(I-1)(I+2)]^{1/2} & 0 \\ -a_p[(I-1)(I+2)]^{1/2} & I(I+1)-1 & 1 & -a_p[I(I+1)]^{1/2} \\ -a_p[(I-1)(I+2)]^{1/2} & 1 & -I(I+1)-1 & -a_p[I(I+1)]^{1/2} \\ 0 & -a_p[I(I+1)]^{1/2} & -a_p[I(I+1)]^{1/2} & I(I+1) \end{pmatrix},$$

where $A(I) = \frac{1}{2(J_0+J_1\omega^2)}$, with the moment of inertia parameter values $J_0 = 7.7\hbar^2$ MeV^{-1} and $J_1 = 83.3\hbar^4$ MeV^{-3}, which were the same as those used in the particle-rotor model calculation. The rotational frequency ω for each angular momentum $I\hbar$ was calculated from the expression $I = i_0 + J_0\omega + J_1\omega^3$, where the value of the alignment parameter i_0 was taken to be 3.6. This value was obtained from the experimental level scheme of ^{132}La. For the decoupling parameter a_p, a value of 4.5 was used for a proton in the low Ω orbit of $h_{11/2}$. The above matrix was diagonalized to find the lowest eigenvalue for each I. The results are compared with the experimental energy levels in Fig. 7(a), designated as "The. II."

As far as the calculation for ^{131}La was concerned, the pseudospin coupling model could not be used because of the absence of a valence neutron above the even-even core nucleus ^{130}Ba.

The pseudospin coupling model was also utilized for ^{131}Ba considering the same model space $[\widetilde{411}\frac{1}{2}]$, $[\widetilde{411}\frac{3}{2}]$ for the valence neutron. In this case, the following 2×2 matrix was used:

$$A(I)\begin{pmatrix} I(I+1) & -[I(I+1)]^{1/2} \\ -[I(I+1)]^{1/2} & I(I+1) \end{pmatrix}.$$

This matrix was diagonalized to get the lowest eigenvalues for each I. The values of the parameters J_0, J_1 were taken to be the same as above. The value of ω for each I was obtained by using $i_0 = 0$ for the ground-state positive-parity band of ^{131}Ba. The calculated energy levels are compared with the experiment in Fig. 7(c), designated as "The. II."

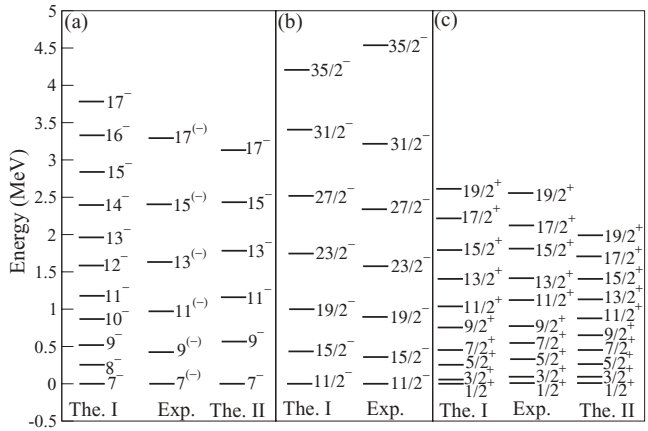

FIG. 7. A comparison of the decoupled band 2 belonging to ^{132}La with the theoretical calculations based on particle-rotor model (The. I) and pseudospin coupling model (The. II) is shown in panel (a). Panels (b) and (c) show a similar comparison for ^{131}La and ^{131}Ba, respectively.

We discuss here the theoretical results in comparison with the experimental data shown in Fig. 7. The results from the particle-rotor model were quite good for ^{131}Ba and ^{131}La. However, the levels predicted by the pseudospin coupling model did not match well with the experiment for ^{131}Ba. For ^{132}La, the theory of a particle-rotor model overpredicted the energy of the levels, particularly at high spins. Also there was a very small signature splitting in the theoretical prediction. This was not consistent with the double decoupling behavior in general, when the large signature splitting was expected and the unfavored component was not observed as it was high in energy. To explain the absence of even-parity states (unfavored signature) in our experimental data, we calculated the decay rates using the particle-rotor model. The values were found to be in the range of 0.1–0.4 ps^{-1} for all the states belonging to both favored as well as unfavored states. The $M1$ transitions from the even-parity states to odd-parity states were also of similar strength. However, the $M1$ transitions from the odd-parity states to even-parity states were found to be very weak with a decay rate of about 0.001 ps^{-1}. Therefore, the γ-ray intensities in the unfavored branch was expected to be much smaller than that in the favored branch. In the pseudospin coupling model, Kreiner [23] has explained such semidecoupled behavior in ^{186}Ir by considering the alignment of a proton spin and a neutron pseudospin. The $M1$ transition strengths between favored (odd spin) and unfavored (even spin) energy states were expected to be very small. However, with the much more powerful detector array GASP, the weakly populated unfavored signature band was observed [6].

V. CONCLUSION

From our earlier measurement we experimentally identified band 2 [11]. The spin $7^{(-)}$ was assigned to the bandhead. Only one signature band with odd spins was observed. In the present work, the RDM technique was utilized to measure the lifetime of states in the picosecond range. From the measured lifetimes of two states, the deformation parameter β has been found to be 0.18. This band showed the decoupled behavior because of the similar energy-level spacings to those of the neighboring nuclei ^{131}La and ^{130}Ba. Two theoretical approaches, the particle-rotor model and the pseudospin coupling model, were used to do a systematic investigation of ^{131}La, ^{131}Ba, and ^{132}La. Considering the valence proton, neutron configuration as $(\pi h_{11/2})$, $(\nu d_{3/2}s_{1/2})$ in the particle-rotor calculation, the energy levels of ^{131}La and ^{131}Ba were found to be matching very well with the experiment. However, for ^{132}La, the calculation produced somewhat larger spacings as compared to the experiment. In the framework of pseudospin coupling model with the coupling of $\pi h_{11/2}$ and $[\widetilde{411}\frac{1}{2}]$, $[\widetilde{411}\frac{3}{2}]$, the energy levels of ^{132}La were well reproduced. Both the models suggested that the intensity of the unfavored signature band should be much smaller than that in the favored band. This explained the absence of even-parity states in the experimental decay scheme.

ACKNOWLEDGMENTS

The authors would like to thank Dr. I. Ragnarsson for providing the particle-rotor model code and some useful discussions. The authors are also thankful to Professor R. Varma, Dr. Richa Jain, and Dr. Ankhi Ray for their help during the experiment. The help provided by Deepa Thapa and S. Mahadkar in preparing the targets is gratefully acknowledged. The full cooperation of the Pelletron staff at IUAC and TIFR for the smooth running of the experiments is also thankfully acknowledged. This work was supported by a research grant (Project No. HR/OY/P-04/97) from Department of Science and Technology, Government of India. The financial support to Vinod Kumar from the Council of Scientific and Industrial Research, New Delhi, is gratefully acknowledged.

APPENDIX

Here we present a brief description of the fitting procedure for finding the lifetimes using a multilevel decay scheme. Let us consider four levels, A, B, C, and D, with A at the top and D at the bottom. The total decay rates for the levels A, B, and C are λ_A, λ_B, and λ_C, respectively. If from the level A, f_A is the fractional decay going to B, the corresponding γ transition will have the partial level width $f_A\lambda_A$. Similarly, the partial level widths for the γ transitions from B to C and from C to D are $f_B\lambda_B$ and $f_C\lambda_C$, respectively. The decay rates for the side feed to the levels B and C are λ_{BI} and λ_{CI}, respectively. The fraction of the side-feeding intensity to the levels B and C are F_B and F_C, respectively. Lifetimes of the levels that were lying higher than two levels above a given state were assumed to have a negligible contribution to the time dependence of that state. In this decay scheme, the expression for the ratio of unshifted γ-ray intensity, $I_0(t)$, and total intensity, $I_0(t) + I_s(t)$, for the γ transition decaying from the level C to D is given as

$$\frac{I_o(t)}{I_o(t) + I_s(t)} = \frac{1}{f_B f_A(1 - F_B - F_C) + f_B F_B + F_C}$$

$$\times\left[\frac{\lambda_A\lambda_B\lambda_C f_A f_B(1-F_B-F_C)}{(\lambda_A-\lambda_B)}\left(\frac{e^{-\lambda_C t}}{\lambda_C(\lambda_B-\lambda_C)}\right.\right.$$
$$-\frac{e^{-\lambda_B t}}{\lambda_B(\lambda_B-\lambda_C)}-\frac{e^{-\lambda_C t}}{\lambda_C(\lambda_A-\lambda_C)}+\left.\frac{e^{-\lambda_A t}}{\lambda_A(\lambda_A-\lambda_C)}\right)$$
$$+\frac{\lambda_B\lambda_C f_B\lambda_{BI}F_B}{(\lambda_{BI}-\lambda_B)}\left(\frac{e^{-\lambda_C t}}{\lambda_C(\lambda_B-\lambda_C)}-\frac{e^{-\lambda_B t}}{\lambda_B(\lambda_B-\lambda_C)}\right.$$
$$-\frac{e^{-\lambda_C t}}{\lambda_C(\lambda_{BI}-\lambda_C)}+\left.\frac{e^{-\lambda_{BI} t}}{\lambda_{BI}(\lambda_{BI}-\lambda_C)}\right)$$
$$+\frac{\lambda_C\lambda_{CI}F_C}{(\lambda_C-\lambda_{CI})}\left(\frac{e^{-\lambda_{CI} t}}{\lambda_{CI}}-\frac{e^{-\lambda_C t}}{\lambda_C}\right)\Bigg], \quad \text{(A1)}$$

where $t \equiv \frac{D}{v_{\text{avg.}}}$, D is the target-stopper separation, and $v_{\text{avg.}}$ is the average velocity of the recoiling nuclei. In order to fit the above expression to the experimental data, f_A, f_B, F_B, and F_C were kept fixed and their values were obtained from the experimental γ-ray intensities. The decay rates λ were treated as adjustable parameters in general. But once the decay rate of a given upper level was available, its value was held constant in the subsequent fitting process involving a lower state. For example, while determining the decay rate λ_C from the above expression, λ_A, λ_B, λ_{BI}, and λ_{CI} were kept constant if their values were already determined, otherwise they were varied within a certain range to obtain the best fit. This range was decided on the basis of the experimentally observed shifted and unshifted components of γ-ray intensities. The unobserved side-feeding transitions are assumed to be very fast. In this way, the lifetimes of the states with interconnecting transitions were obtained in a consistent fashion.

[1] K. Starosta, T. Koike, C. J. Chiara, D. B. Fossan, and D. R. LaFosse, Nucl. Phys. A **682**, 375c (2001).
[2] C. M. Petrache *et al.*, Phys. Rev. C **65**, 054324 (2002).
[3] F. G. Kondev *et al.*, Phys. Rev. C **59**, 3076 (1999).
[4] R. Wadsworth, S. M. Mullins, P. J. Bishop, A. Kirwan, M. J. Godfrey, P. J. Nolan, and P. H. Regan, Nucl. Phys. A **526**, 188 (1991).
[5] A. J. Kreiner *et al.*, Phys. Rev. C **50**, R530 (1994).
[6] M. A. Cardona *et al.*, Phys. Rev. C **55**, 144 (1997).
[7] C. Gerschel and N. Perrin, Compt. Rend. B **269**, 220 (1969).
[8] J. R. B. Oliveira, L. G. R. Emediato, M. A. Rizzutto, R. V. Ribas, W. A. Seale, M. N. Rao, N. H. Medina, S. Botelho, and E. W. Cybulska, Phys. Rev. C **39**, 2250 (1989).
[9] K. Starosta, C. J. Chiara, D. B. Fossan, T. Koike, T. T. S. Kuo, D. R. LaFosse, S. G. Rohoziński, Ch. Droste, T. Morek, and J. Srebrny, Phys. Rev. C **65**, 044328 (2002).
[10] K. Starosta *et al.* Phys. Rev. Lett. **86**, 971 (2001).
[11] V. Kumar, P. Das, R. P. Singh, S. Muralithar, and R. K. Bhowmik, Eur. Phys. J. A **17**, 153 (2003).
[12] J. Timár *et al.*, Eur. Phys. J. A **16**, 1 (2003).
[13] E. Grodner *et al.*, Int. J. Mod. Phys. E **14**, 347 (2005).
[14] T. K. Alexander and J. S. Forster, in *Advances in Nuclear Physics*, edited by M. Baranger and E. Vogt (Plenum, New York, 1978), Vol. 10, Chap. 3.
[15] H. C. Jain, S. Chattopadhyay, Y. K. Agarwal, M. L. Jhingan, S. K. Mitra, H. V. Panchal, and A. Roy, Pramana **37**, 269 (1991).
[16] S. C. Pancholi and R. K. Bhowmik, Indian J. Pure Appl. Phys. **27**, 660 (1989).
[17] D. C. Radford, Nucl. Instrum. Methods Phys. Res. A **361**, 297 (1995).
[18] A. Bohr and B. R. Mottelson, *Nuclear Structure* (Benjamin, New York, 1975), Vol. II.
[19] P. Ring and P. Schuck, *The Nuclear Many Body Problem* (Springer-Verlag, Heidelberg, 1980).
[20] S. E. Larsson, G. Leander, and I. Ragnarsson, Nucl. Phys. A **307**, 189 (1978).
[21] R. Ma, Y. Liang, E. S. Paul, N. Xu, D. B. Fossan, L. Hildingsson, and R. A. Wyss, Phys. Rev. C **41**, 717 (1990).
[22] A. Bohr, I. Hamamoto, and Ben R. Mottelson, Phys. Scr. **26**, 267 (1982).
[23] A. J. Kreiner, Phys. Lett. B **279**, 233 (1992).